Effective modeling of magnitude-fluctuated magnetization dynamics: Dynamic precursor effect in magnets

Yu Wang [1,*] Jie Wang,[2,3] Takayuki Kitamura,[1] Hiroyuki Hirakata,[1] and Takahiro Shimada[1]

[1]*Department of Mechanical Engineering and Science, Kyoto University, Nishikyo-ku, Kyoto 615-8540, Japan*
[2]*Department of Engineering Mechanics, Zhejiang University, Hangzhou 310027, China*
[3]*Zhejiang Laboratory, Hangzhou 311100, China*

Effective modeling of magnetization dynamics is key to understanding the nature of exotic magnetic structures and behaviors such as magnetic skyrmions and spin waves. Although the modeling of magnitude variation of magnetizations is crucial for magnets at finite temperatures (especially near the Curie temperature with the precursor effect), it is restrained in common micromagnetic simulations. Here, we propose an effective methodology for modeling the magnitude-fluctuated magnetization dynamics based on Ginzburg-Landau theory, which includes both the precession motion and adjustable magnitude of magnetizations simultaneously. Our model includes the intrinsic synergy of precession motion and adjustable magnitude of magnetizations, i.e., dynamic precursor effect. Therefore, in this paper, we provide an advanced simulation methodology and introduce an intrinsic dynamic modulation in magnetic system, which is anticipated to be a starting point for the future study of the dynamics of magnetization, magnetic domains, and topologies in magnets.

I. INTRODUCTION

Magnetization **M** is a vector that expresses the density of magnetic moments in a continuum model [1,2], and a region with uniform direction of magnetizations is called a *magnetic domain* [1,3]. Topological magnetic structures like skyrmions [4,5] are topological stable magnetic domains with specific configurations of magnetizations. They are all scientifically significant due to their promising dynamic applications in spintronics [6–9]. The dynamic behaviors of magnetizations, magnetic domains, and topologies under physical fields are generally described by the Landau-Lifshitz-Gilbert (LLG) [10–12] equation, which shows the precessional motion of magnetizations. However, in LLG equation-based simulations, the constant temperature assumption [13–20] is widely used for numerical implementation, in which the magnitude of magnetization $|\mathbf{M}|$ is constrained to a constant and only considers the direction of the unit vector of magnetization **m**. However, the Ginzburg-Landau theory [1] demonstrated that the magnetization magnitude $|\mathbf{M}|$ can be changed by physical fields (such as temperature). Especially the adjustable magnitude of magnetization is reported to be crucial near the Curie temperature, where magnetizations become soft, i.e., easy to change in magnitude, due to the precursor effect [4,21]. The magnetization magnitude therefore even becomes inhomogeneous in space, which forms more complicated magnetic domains [22,23]. Therefore, the variation of magnetization magnitude is nonnegligible. In the literature, there are two popular ways to address the variation of magnetization magnitude in magnetic simulations. One

way is changing the LLG equation to the Landau-Lifshitz-Bloch (LLB) form [24–28] by adding a thermal stochastic field into the discrete spin model, which is from the view of microscopic quantum theory. However, the precursor effect is introduced by the continuum magnetization model from the thermodynamic macroscopic theory [4]. Therefore, the other way comes out by reducing the LLG equation to the time-dependent Ginzburg-Landau (TDGL) form [29–31] in the continuum model based on the overdamped assumption [30,32–37], but it neglects the precession motion of magnetizations [38], thereby lacking accuracy in dynamic scenarios. Thus, to simulate the precursor effect in dynamic scenarios, introducing the macroscopic Ginzburg-Landau theory into the LLG equation with less restraint, then simultaneously describing the magnitude variation of magnetizations, the precursor effect, and the precessional nature of magnetization dynamics in a continuum model is the aim of this paper.

II. RESULTS AND DISCUSSIONS

We start our discussion in detail. The general LLG equation [10–12] can be written as

$$\frac{\partial \mathbf{M}}{\partial t} = -\gamma_1 \mathbf{M} \times \mathbf{H}_{\text{eff}} - \gamma_2 \mathbf{M} \times (\mathbf{M} \times \mathbf{H}_{\text{eff}}), \quad (1)$$

where $\gamma_1 = \gamma/(1 + \alpha^2)$, $\gamma_2 = \alpha\gamma/[(1 + \alpha^2)M_s]$ (γ is the gyromagnetic ratio, α is the Gilbert damping, M_s is the saturated magnetization), $\mathbf{H}_{\text{eff}} = (-1/\mu_0)(\delta F/\delta \mathbf{M}) = (-1/\mu_0)[(\partial f/\partial M_i) - (\partial/\partial x_j)(\partial f/\partial M_{i,j})]$ is the effective magnetic field [33,35], and $F = \int f dv$ is the total free energy, in which f is the free energy density [33]. The free energy density of a ferromagnetic system with the Dzyaloshinskii-Moriya interaction (DMI) [39,40] is generally

*wang.yu.51p@st.kyoto-u.ac.jp

expressed as

$$f = f_{Landau} + f_{exchange} + f_{DM} + f_{magnetic} + f_{elastic}, \quad (2)$$

where f_{Landau}, $f_{exchange}$, f_{DM}, $f_{magnetic}$, and $f_{elastic}$ are the Landau, exchange, DMI, magnetostatic, and elastic energy densities, respectively. The detailed forms of them are shown in Appendix A. Particularly, the Landau energy density [1,4,41] is presented by the Ginzburg-Landau theory [1] to reveal the temperature-controlled magnitude of magnetizations, which is the theory basis of the precursor effect [4,21] and the second-order phase transition of magnetization [1,42–46]. It can be written as

$$f_{Landau} = a(T - T_c)\mathbf{M}^2 + b\mathbf{M}^4, \quad (3)$$

where a and b are the Landau energy coefficients, T is temperature, and T_c is the Curie temperature. Therefore, to realize the aim of this paper, the Landau energy density f_{Landau} should be included in the LLG equation via the effective field $\mathbf{H}_{eff}$. However, the Landau energy-induced effective field $\mathbf{H}_{eff}^{Landau}$ always makes the gyromagnetic term $\mathbf{M} \times \mathbf{H}_{eff}^{Landau}$ of the LLG equation equal to zero, which leads to the general LLG equation constraining the magnitude of magnetization and makes it a technical challenge for describing the magnitude variation in magnetization dynamics. Therefore, two common assumptions are introduced for this problem in the literature. One is the constant temperature assumption [13], i.e., the magnitude of magnetization is constrained to saturated magnetization ($|\mathbf{M}| = M_s$), and only the unit vector of magnetization $\boldsymbol{m}$ is solved in the LLG equation [15,16,18,19,47], in which the temperature effect and the variation of magnetization magnitude are totally neglected. The other assumption is the overdamped assumption [32,33,35], which exaggerates the damping motion [γ_2 term in Eq. (1)] and neglects the precession of magnetizations [γ_1 term in Eq. (1)]. With this assumption, the LLG equation can be reduced to the form of the TDGL equation [29,30] as

$$\frac{\partial \mathbf{M}}{\partial t} = -L \frac{\delta F}{\delta \mathbf{M}}, \quad (4)$$

where $L = \gamma M_s / \alpha \mu_0$ is the kinetic coefficient for magnetization evolution. By this method, the field-controlled magnitude of magnetization and the precursor effect are included in the simulation (without the neutralizing of $\mathbf{M} \times \mathbf{H}_{eff}^{Landau} = 0$), but the precessional nature of magnetization is abandoned, which is unconscionable in the dynamic scenarios. Therefore, both previous assumptions are inappropriate for magnetization dynamics and may even reach unconscionable configurations of magnetic domains due to strong confines of the evolution process and magnitude of magnetizations. For example, a 90° change of moving direction has been reported in a current-driven skyrmion due to the precessional nature of magnetization [48]. The inhomogeneous physical field-induced skyrmion motion has been demonstrated to be related to the magnetization magnitude [33]. Near the Curie temperature, a new skyrmionic A phase occurs due to the softening of the magnetization magnitude by the precursor effect [22,23].

To get closer to the dynamic behaviors of magnetization with the precursor effect, the Landau energy needs to be implemented in the LLG equation without neglecting the precessional gyromagnetic term. Here, by using the relation-

ship of $\mathbf{a} \times (\mathbf{b} \times \mathbf{c}) = (\mathbf{a} \cdot \mathbf{c})\mathbf{b} - (\mathbf{a} \cdot \mathbf{b})\mathbf{c}$, the LLG equation Eq. (1) can be written as

$$\frac{\partial \mathbf{M}}{\partial t} = -\gamma_1 \mathbf{M} \times \mathbf{H}_{eff} - \gamma_2 (\mathbf{M} \cdot \mathbf{H}_{eff})\mathbf{M} + \gamma_2 \mathbf{M}^2 \mathbf{H}_{eff}. \quad (5)$$

On the right side of Eq. (5), the first term is the gyromagnetic term, which describes the precession velocity of magnetization; the second term shows the longitudinal velocity of magnetization associated with precession motion [31]; and the third term represents the damping effect, which drives the magnetization in the direction of the effective field, i.e., effective field-driven velocity. Thereby, the variation of the magnetization magnitude $|\mathbf{M}|$ can be driven by the longitudinal velocity of magnetization (in the second term) and by the effective field (in the third term). However, magnitude change driven by the effective field (via thermodynamic free energy) is assumed much more dominant than being driven associated with magnetization precession [31]. Therefore, here, we adopt that the variation of the magnetization magnitude is only controlled by the free energy inside the effective field in our methodology. Mathematically, it is stated as

$$\gamma_2 (\mathbf{M} \cdot \mathbf{H}_{eff})\mathbf{M} = 0. \quad (6)$$

By applying this assumption in Eq. (5), the modified equation for the magnetic dynamics is yielded as

$$\frac{\partial \mathbf{M}}{\partial t} = -\gamma_1 \mathbf{M} \times \mathbf{H}_{eff} + \gamma_2 \mathbf{M}^2 \mathbf{H}_{eff}. \quad (7)$$

Equation (7) breaks the limitation of constrained magnetization magnitude and keeps both precession and damping motions of magnetizations. Meanwhile, the temperature- and magnetization magnitude-related Landau energies can be implemented in the damping γ_2 term without neutralizing. Therefore, it is expected to become a promising governing equation of the magnetization dynamics, which can reflect the precession motion, damping motion, variation of magnetization magnitude, and the temperature-related precursor effect at the same time.

Then a steady-state motion of magnetic domains is employed to check the reliability of the assumption and Eq. (7) analytically. The dynamic properties of magnetic domains are mathematically described by a kinetic equation, i.e., the Thiele equation [49], which is derived from the general LLG equation. With our assumption, the Thiele equation of Eq. (7) is derived accordingly as follows. Taking the cross-product of Eq. (7) with the magnetization $\mathbf{M}$ leads to

$$\mathbf{M} \times \left(\frac{\partial \mathbf{M}}{\partial t} + \gamma_1 \mathbf{M} \times \mathbf{H}_{eff} - \gamma_2 \mathbf{M}^2 \mathbf{H}_{eff} \right) = 0. \quad (8)$$

Therefore, we have

$$\mathbf{M} \times \mathbf{H}_{eff} = \frac{1}{\gamma_2 \mathbf{M}^2} \mathbf{M} \times \frac{\partial \mathbf{M}}{\partial t}$$
$$- \frac{\gamma_1}{\gamma_2 \mathbf{M}^2} [(\mathbf{M} \cdot \mathbf{H}_{eff})\mathbf{M} - \mathbf{M}^2 \mathbf{H}_{eff}]. \quad (9)$$

Substituting Eq. (9) into Eq. (8) yields

$$\mathbf{M} \times \left(\frac{\alpha}{\gamma M_s} \frac{\partial \mathbf{M}}{\partial t} + \frac{1}{\gamma M_s^2} \mathbf{M} \times \frac{\partial \mathbf{M}}{\partial t} - \mathbf{H}_{eff} \right) = 0. \quad (10)$$

This means that the magnetization $\mathbf{M}$ is parallel to the vector of the bracket, which means spatial derivatives of the magnetization $\mathbf{M}$ are perpendicular to this vector [50]:

$$\frac{\partial \mathbf{M}}{\partial x_i} \cdot \left(\frac{\alpha}{\gamma M_s} \frac{\partial \mathbf{M}}{\partial t} + \frac{1}{\gamma M_s^2} \mathbf{M} \times \frac{\partial \mathbf{M}}{\partial t} - \mathbf{H}_{\text{eff}} \right) = 0, \quad (11)$$

or in Einstein notation:

$$\frac{\partial M_k}{\partial x_i} \cdot \left(\frac{\alpha}{\gamma M_s} \frac{\partial M_k}{\partial t} + \frac{1}{\gamma M_s^2} e_{jlk} M_j \frac{\partial M_l}{\partial t} - H_k^{\text{eff}} \right) = 0, \quad (12)$$

where e_{jlk} is the permutation symbol. For the steady motion of the magnetic domain [49] with velocity v_j, there are

$$M_i = M_i(x_j - X_j), \quad (13a)$$

$$X_j = v_j t, \quad (13b)$$

$$\frac{\partial M_i}{\partial t} = -\frac{v_j \partial M_i}{\partial x_j}, \quad (13c)$$

where x_j are field positions, and X_j are magnetic domain positions. By using Eq. (13), Eq. (12) can be written as

$$-\frac{\alpha}{\gamma M_s} \frac{\partial M_k}{\partial x_i} \frac{\partial M_k}{\partial x_j} v_j - \frac{1}{\gamma M_s^2} e_{jlk} M_j \frac{\partial M_k}{\partial x_i} \frac{\partial M_l}{\partial x_n} v_n$$
$$- H_k^{\text{eff}} \frac{\partial M_k}{\partial x_i} = 0. \quad (14)$$

Substituting the driving force density [49–51] on the magnetic domain $f_i = -H_k^{\text{eff}} \partial M_k / \partial x_i$ into Eq. (14), we derive

$$-\frac{\alpha}{\gamma M_s} \frac{\partial M_k}{\partial x_i} \frac{\partial M_k}{\partial x_j} v_j - \frac{1}{\gamma M_s^2} e_{jlk} M_j \frac{\partial M_k}{\partial x_i} \frac{\partial M_l}{\partial x_n} v_n + f_i = 0. \quad (15)$$

The dissipation matrix and gyrocoupling vector are defined by Thiele [49] as

$$d_{ij} = \left(-\frac{\alpha}{\gamma M_s} \right) \left(\frac{\partial M_k}{\partial x_i} \right) \frac{\partial M_k}{\partial x_j}, \quad (16a)$$

$$g_m = \left(-\frac{1}{\gamma M_s^2} \right) \delta_{jlk}^{mni} M_j \left(\frac{\partial M_k}{\partial x_i} \right) \frac{\partial M_l}{\partial x_n}, \quad (16b)$$

where $\delta_{jlk}^{mni} = e_{mni} e_{jlk}$ is a generalized Kronecker symbol. With the definition of Eq. (16), Eq. (15) can be written as

$$d_{ij} v_j + e_{mni} g_m v_n + f_i = 0, \quad (17)$$

which can be expressed by vector notation as

$$\mathbf{d} \cdot \mathbf{v} + \mathbf{g} \times \mathbf{v} + \mathbf{f} = 0. \quad (18)$$

Obviously, Eq. (18) is the conventional Thiele equation for the magnetic domain motion [49]. It has a consistent form with the kinetic equation derived from the general LLG equation analytically and clearly shows the gyrocoupling and dissipation velocities of the magnetic domain under a driving force. This result demonstrates that the assumption we adopted in this paper [Eq. (6)] indeed does not influ-

TABLE I. Material parameters of MnSi [32–34,41,57–59].

Landau energy coefficients		Curie temperature	
a_0	6.44×10^{-7} JA^{-2} m^{-1} K^{-1}	T_c	29.5 K
b	3.53×10^{-16} Jm A^{-4}		
Exchange energy coefficient		DMI constant	
A	$1.27 \times 10{-}23$ Jm A^{-2}	D	1.14×10^{-14} J/A^2
	Vacuum permeability		Saturated magnetization
μ_0	$4\pi \times 10^{-7}$ Hm^{-1}	M_s	1.63×10^5 A/m
	Elastic constants		Magnetostrictive coefficients
C_{11}	2.83×10^{11} J/m^3	λ_{100}	3.04×10^{-6}
C_{12}	0.64×10^{11} J/m^3	λ_{111}	2.26×10^{-6}
C_{44}	1.17×10^{11} J/m^3		
	Gyromagnetic ratio		Damping
γ	2.2×10^5 m/(As)	α	Mentioned in main text

ence the steady motion of magnetic domains. It implies that the methodology of this paper is suitable for the dynamics of magnetic topologies (like skyrmions), which can be regarded as steady motion due to their topological stable structures [52].

To further verify the accuracy of our methodology for the case that the Thiele equation cannot cover, the numerical results of magnetization switching are discussed subsequently. By a finite element method, we solved Eq. (7), along with the mechanical equilibrium equation:

$$\frac{\partial \sigma_{ij}}{\partial x_j} = \frac{\partial}{\partial x_j} \left(\frac{\partial f}{\partial \varepsilon_{ij}} \right) = 0, \quad (19)$$

and Maxwell's equation:

$$\frac{\partial B_i}{\partial x_i} = \frac{\partial}{\partial x_i} \left(-\frac{\partial f}{\partial H_i} \right) = 0, \quad (20)$$

where σ_{ij}, ε_{ij}, B_i, and H_i are stress, strain, magnetic induction, and magnetic field, respectively. Ferromagnetic MnSi is chosen as an example material for all simulations in this paper. The detail of the finite element method is shown in Appendix B, and the material parameters are shown in Table I.

At first, the trajectory of a single magnetization switching under an external magnetic field is simulated. As shown in the schematic in Fig. 1(a), at the temperature of 0 K, the
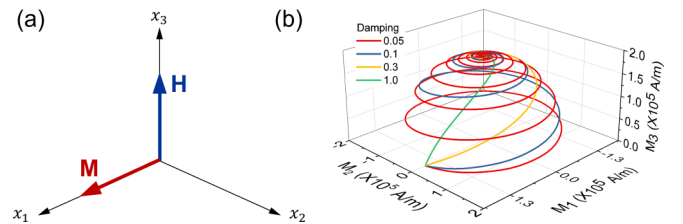

FIG. 1. (a) Schematic of the initial position of the magnetization and the direction of the external magnetic field. (b) Trajectories of magnetizations under an external magnetic field with different damping at 0 K.
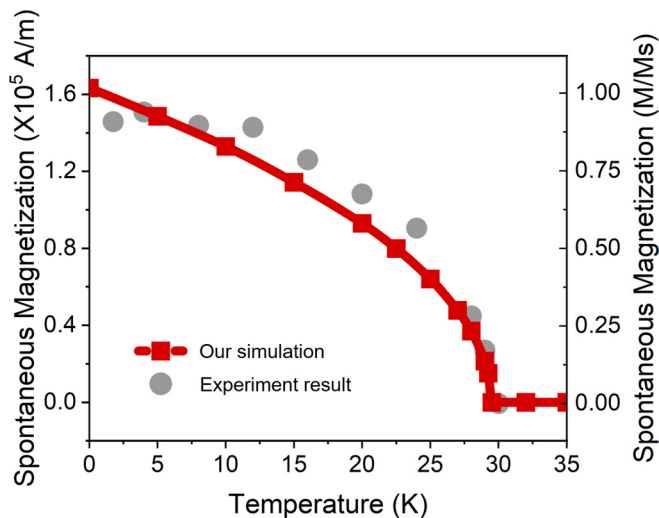
FIG. 2. Relationship of spontaneous magnetizations and temperatures (M-T curve). Red line with squares is the result of our simulation (left y axis), and gray dots are the normalized experimental results from Ref. [46] (right y axis).

initial position of the magnetization is parallel to the x_1 direction, with the spontaneous magnitude of 1.63×10^5 A/m. Then an external magnetic field is applied along the x_3 direction as $H_3 = 20 \times 10^5$ A/m. As the simulated results show in Fig. 1(b), under the excitation of the external field, the magnetization starts to move toward the direction of the magnetic field. Specifically, the magnetization has precession rotation due to its gyromagnetic nature, and it approaches the external field by the damping effect gradually until it is parallel to the external field as the stable state. In addition, when the damping α is increased from 0.05 to 1.0, the approaching process of the magnetization is faster, and the precession of it is suppressed accordingly. These results clearly show the precession and damping nature of the magnetization motion.

Next, to show the magnetization magnitude-related Landau energy is physically sound in the simulation without neutralizing, the spontaneous magnetization at different temperatures is simulated and shown in Fig. 2. The red line with squares is the result of our simulation; it reproduced well the analytical value of the Landau theory, and the gray dots are the experimental results as a comparison. The details of the comparisons of the results between the Landau theory, experiment, microscopic model, and our simulation model are shown in the Supplemental Material [53]. As shown in Fig. 2, it accurately reveals the phenomenon that the spontaneous magnetization decreases with the increase of temperature and vanishes at the Curie temperature of 29.5 K for MnSi, which is consistent with the second-order phase transition from ferromagnetic to paramagnetic phase [1,46]. Therefore, our simulation model reveals the magnetization magnitude change in finite temperatures well by the Landau theory and magnetic dynamic equation.

Further, in addition to the spontaneous magnetization related to the system temperature, the magnetization magnitude is also controlled by other physical fields such as external magnetic field or strain field [54]. The well-known evi-

dence is the magnetic field-induced magnetization above the Curie temperature, in which the spontaneous magnetization is absent. Therefore, the magnetization-magnetic field ($M-H$) curves at different temperatures are simulated by our model in Fig. 3(a). The result demonstrates the magnetic field-controlled magnetization is revealed at finite temperatures. Especially the external magnetic field-induced magnetization in the paramagnetic state at 30 K is predicted [the green line in Fig. 3(a)]. Meanwhile, Fig. 3(b) shows the magnetostrictive strain induced by magnetic fields in different temperature fields. They further demonstrated that the magnetization magnitude can be controlled by the competition of multiphysics fields such as temperature, magnetic, and strain fields. This result demonstrates that the methodology successfully includes the adjustable magnitude of magnetization by the thermodynamic Ginzburg-Landau theory.

In the end, to compare with other existing methodologies, Fig. 4 shows the magnetization switching trajectories in methodologies with different assumptions, i.e., (a) the constant temperature assumption, (b) the overdamped assumption, and (c) the assumption of this paper. Like Fig. 1, the initial magnetization in Fig. 4 is along the x_1 direction, and it is driven by an external magnetic field in the x_3 direction. At first, Fig. 4(a) shows the magnetization trajectory calculated with a constant temperature assumption [55,56]. It is the representative result for existing micromagnetic simulations [13,47], which constrain the magnetization magnitude. It clearly shows the precession and damping motion of a magnetization but cannot consider the variation of the magnetization magnitude, in which the confined magnetization only moves on a sphere with a constant magnitude. Then Fig. 4(b) shows the magnetization trajectory calculated with an overdamped assumption by the TDGL form of the equation. It indeed reflects the variation of the magnetization magnitude in different temperatures but neglects the precession of magnetization. Next, Fig. 4(c) shows the result from the methodology of this paper. Here, the precession and damping motion of magnetization are well simulated, and at the same time, the magnitude evolution of magnetizations is soundly reflected, i.e., the magnetization magnitude is governed by temperature and magnetic fields. The magnetization is no longer restrained in a constant sphere like Fig. 4(a).

Further, in Fig. 4(c), the magnetization magnitude is hard to change at 0 K (red line), while it becomes soft near the Curie temperature. The magnitude change by the magnetic field is 82.2% at 29 K (green line), which clearly reveals the precursor effect (detailed in the Supplemental Material [53]). This result demonstrates that our model successfully simulated the precursor effect and the precession motion of magnetization at the same time. Therefore, the diverse trajectories of magnetization can be created by the synergy of precession motion and adjustable magnitude of magnetizations. This result indicates that the precessional nature of magnetization along with the precursor effect may create more complicated evolution processes and configurations of magnetizations, which can be named as the *dynamic precursor effect*. With this intrinsic dynamic modulation of magnetizations, several magnetization behaviors that were previously suppressed will emerge, especially near the Curie temperature.
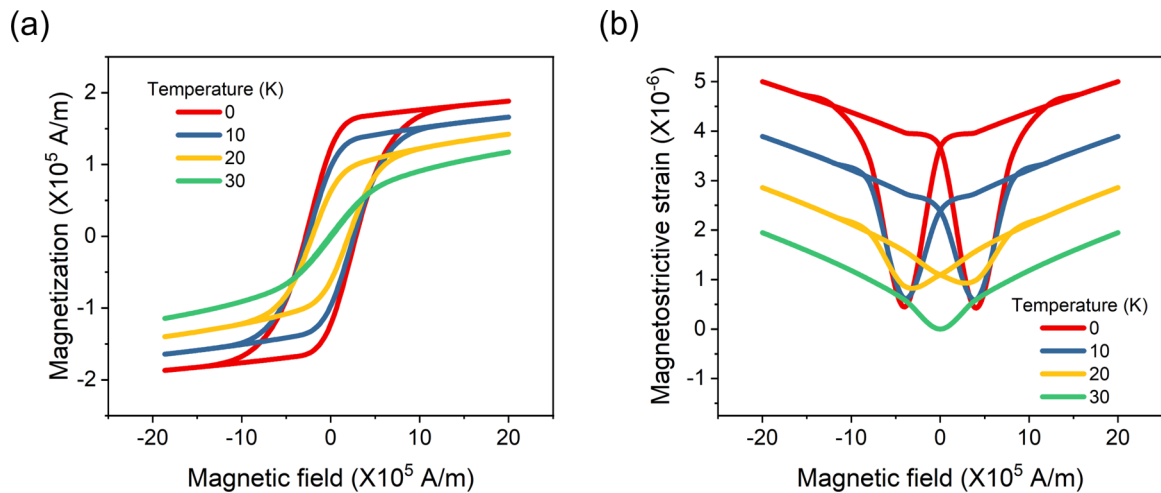
(a)

(b)

FIG. 3. (a) M-H curves in different temperatures. The saturation magnetization under external magnetic field at 0, 10, 20, and 30 K are 1.8834, 1.6617, 1.424, and 1.175×10^5 A/m, respectively. (b) Magnetostrictive strain-magnetic field curves in different temperatures.
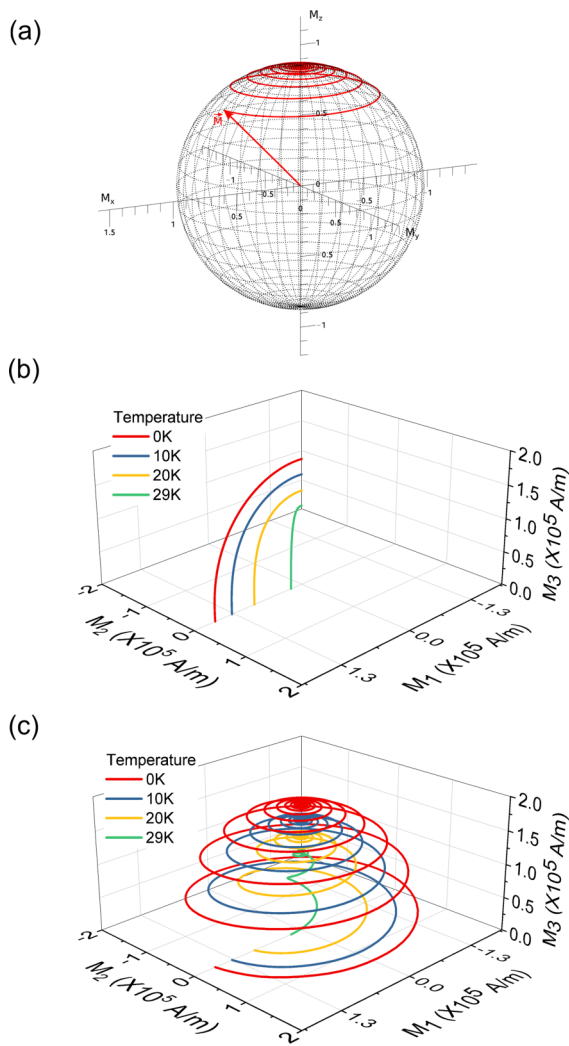
(a)

(b)

(c)

FIG. 4. (a) Trajectory of magnetization by the constant temperature assumption from Ref. [52]. (b) Trajectory of magnetization by the overdamped assumption. (c) Trajectory of magnetization by the assumption of this paper.

III. CONCLUSIONS

In summary, we combined the Ginzburg-Landau theory and the LLG equation to realize the synergy of directional motions and the magnitude variation of magnetizations in a continuum model. The analytical deduction demonstrated this model is especially suitable for the dynamics of magnetic topologies (like skyrmions). The numerical simulation shows the methodology can reproduce well multitudinous dynamic motions of magnetizations in physical fields. The trajectory result further indicates the intrinsic dynamic precursor effect can be simulated by the methodology of this paper. In this paper, we provide an advanced magnetic simulation methodology including the dynamic precursor effect, which is an intrinsic modulation for magnetizations. It will trigger a series of phenomena in magnetic dynamic behaviors (such as the unprecedented behaviors of spin waves or skyrmion motions near the Curie temperature), which is a benefit for their application in spintronic devices. Therefore, we anticipate this paper to be an update for existing magnetic simulations to exploit an intriguing avenue for the future research on magnetic dynamics.

ACKNOWLEDGMENTS

APPENDIX A: DETAIL OF FREE ENERGY DENSITY

The total free energy density in the ferromagnetic system [33] can be written as

$$f = f_{\text{Landau}} + f_{\text{exchange}} + f_{\text{DM}} + f_{\text{magnetic}} + f_{\text{elastic}}, \quad \text{(A1)}$$

where f_{Landau}, f_{exchange}, f_{DM}, f_{magnetic}, and f_{elastic} are the Landau, exchange, DMI, magnetostatic, and elastic energy densities, respectively. The Landau energy density

[1,4,32,33], which includes the temperature effect, can be expressed as

$$f_{\text{Landau}} = a(T - T_c)\mathbf{M}^2 + b\mathbf{M}^4, \tag{A2}$$

where a and b are the Landau energy coefficients, T is temperature, and T_c is the Curie temperature. The exchange energy density can be written as

$$f_{\text{exchange}} = A\big(M_{1,1}^2 + M_{1,2}^2 + M_{1,3}^2 + M_{2,1}^2 + M_{2,2}^2 + M_{2,3}^2 \\ + M_{3,1}^2 + M_{3,2}^2 + M_{3,3}^2\big), \tag{A3}$$

where A is the exchange energy coefficient, and $M_{i,j} = \partial M_i / \partial x_j$ denotes the derivative of magnetization M_i with respect to x_j. The bulk-type DMI energy density of MnSi can be expressed as

$$f_{\text{DM}} = D(M_1 M_{3,2} - M_1 M_{2,3} + M_2 M_{1,3} - M_2 M_{3,1} \\ + M_3 M_{2,1} - M_3 M_{1,2}), \tag{A4}$$

where D is the DMI constant. The magnetostatic energy density is written as

$$f_{\text{magnetic}} = -\frac{\mu_0}{2}\big(H_1^2 + H_2^2 + H_3^2\big) \\ - \mu_0(H_1 M_1 + H_2 M_2 + H_3 M_3), \tag{A5}$$

where H_i represents the magnetic field intensity in the material, and μ_0 is the vacuum permeability. The elastic energy density including pure elastic energy density and magnetostrictive energy density, which expresses the magnetostrictive effect, can be written as

$$f_{\text{elastic}} = \tfrac{1}{2}C_{11}\big(\varepsilon_{11}^2 + \varepsilon_{22}^2 + \varepsilon_{33}^2\big) + C_{12}(\varepsilon_{11}\varepsilon_{22} + \varepsilon_{11}\varepsilon_{33} + \varepsilon_{33}\varepsilon_{22}) \\ + 2C_{44}\big(\varepsilon_{12}^2 + \varepsilon_{13}^2 + \varepsilon_{23}^2\big) - \frac{3\lambda_{100}}{2M_s^2}(C_{11} - C_{12}) \\ \times \big(\varepsilon_{11}M_1^2 + \varepsilon_{22}M_2^2 + \varepsilon_{33}M_3^2\big) - \frac{6\lambda_{111}}{M_s^2} \\ \times C_{44}(\varepsilon_{12}M_1 M_2 + \varepsilon_{23}M_3 M_2 + \varepsilon_{13}M_1 M_3), \tag{A6}$$

where C_{11}, C_{12} and C_{44} are the elastic constants, λ_{100} and λ_{111} are the magnetostrictive coefficients, and M_s is the saturated magnetization.

APPENDIX B: FINITE ELEMENT METHOD FOR SOLVING GOVERNING EQUATIONS

The governing equations of our magnetic simulation methodology are the modified LLG equation:

$$\frac{\partial \mathbf{M}}{\partial t} = -\gamma_1 \mathbf{M} \times \mathbf{H}_{\text{eff}} + \gamma_2 \mathbf{M}^2 \mathbf{H}_{\text{eff}}, \tag{B1}$$

the mechanical equilibrium equation:

$$\frac{\partial \sigma_{ij}}{\partial x_j} = \frac{\partial}{\partial x_j}\left(\frac{\partial f}{\partial \varepsilon_{ij}}\right) = 0, \tag{B2}$$

and Maxwell's equation:

$$\frac{\partial B_i}{\partial x_i} = \frac{\partial}{\partial x_i}\left(-\frac{\partial f}{\partial H_i}\right) = 0. \tag{B3}$$

A nonlinear finite element method is employed to solve the above governing Eqs. (B1)–(B3). The weak form of the governing equation is

$$\int_V \left[\frac{\partial f}{\partial \varepsilon_{ij}}\delta\varepsilon_{ij} + \frac{\partial f}{\partial H_i}\delta H_i + \left(-\frac{\gamma_1}{\mu_0}M_j\frac{\partial f}{\partial M_k}e_{jki} + \frac{\partial M_i}{\partial t} + \frac{\gamma_2 \mathbf{M}^2}{\mu_0}\frac{\partial f}{\partial M_i}\right)\delta M_i + \left(-\frac{\gamma_1}{\mu_0}M_l e_{lki}\frac{\partial f}{\partial M_{k,j}} + \frac{\gamma_2 \mathbf{M}^2}{\mu_0}\frac{\partial f}{\partial M_{i,j}}\right)\delta M_{i,j}\right]dV$$

$$= \int_S (t_i \delta u_i + B_{jn_j}\delta\phi_M + \pi_{M_i}\delta M_i)dS, \tag{B4}$$

in which t_i is the traction on the surface, u_i is the mechanical displacement, B_{jn_j} is the normal component of the magnetic induction, ϕ_M is magnetic potential, and $\pi_{M_i} = (\frac{\gamma_2 \mathbf{M}^2}{\mu_0}\frac{\partial f}{\partial M_{i,j}} - \frac{\gamma_1}{\mu_0}M_l e_{lki}\frac{\partial f}{\partial M_{k,j}})n_j$, respectively. Equation (B4) can be expressed in matrix form as

$$\int_V \{\{\delta\varepsilon\}^T[c]\{\varepsilon\} - \{\delta\varepsilon\}^T[Q]\{\mathbf{M}\} - \{\delta\mathbf{H}\}^T[\mu_0]\{\mathbf{H}\} - \{\delta\mathbf{H}\}^T[\mu_0]\{\mathbf{M}\} - \{\delta\mathbf{M}\}^T[D1_\gamma]\{\mathbf{M}\}$$

$$- \{\delta\mathbf{M}\}^T[\mu_\gamma]\{\mathbf{M}\} - \{\delta\mathbf{M}\}^T[e_\gamma]\{\mathbf{M}\} + \{\delta\mathbf{M}\}^T\{\mathbf{M}_{,t}\} + \{\delta\mathbf{M}\}^T[\alpha]\{\mathbf{M}\} + \{\delta\mathbf{M}\}^T[D1]\{\mathbf{M}_{,j}\}$$

$$+ \{\delta\mathbf{M}\}^T[\mu]\{\mathbf{H}\} + \{\delta\mathbf{M}\}^T[e]\{\varepsilon\} - \{\delta\mathbf{M}_{,j}\}^T[A_\gamma]\{\mathbf{M}\} - \{\delta\mathbf{M}_{,j}\}^T[D2_\gamma]\{\mathbf{M}\} + \{\delta\mathbf{M}_{,j}\}^T[A]\{\mathbf{M}_{,j}\}$$

$$+ \{\delta\mathbf{M}_{,j}\}^T[D2]\{\mathbf{M}\}\}dV = \int_S \{\{\delta\mathbf{u}\}^T\{\mathbf{T}\} + B_n\delta\phi_M + \{\delta\mathbf{M}\}^T\{\pi_{\mathbf{M}}\}\}dS. \tag{B5}$$

In the space discretization, an eight-node hexahedral element with 11 degrees of freedom at each node is employed. The degrees of freedom are three displacement components, one magnetic potential, and three magnetization components. The displacement, scalar magnetic potential, and magnetization are derived from the linear interpolation of the quantities of nodal variables in each element, which have the forms as

$$\{\mathbf{u}\} = [N_u]\{\mathbf{u}^I\}, \quad \phi_M = \langle N_\phi\rangle\{\phi_M^I\}, \quad \{\mathbf{M}\} = [N_M]\{\mathbf{M}^I\}, \quad \text{(B6)}$$

where $[N_u]$, $\langle N_\phi\rangle$, and $[N_M]$ are the interpolation function matrices [35]. The quantities of nodal variables are $\{\mathbf{u}^I\}$, $\{\phi_M^I\}$, and $\{\mathbf{M}^I\}$, in which I donates the node number. The strains, magnetic fields, and magnetization gradients are also derived

from the quantities of nodal variables as

$$\{\varepsilon\} = [B_u]\{\mathbf{u}^I\}, \quad \{\mathbf{H}\} = -[B_\phi]\{\phi_M^I\}, \quad \{\mathbf{M}_{i,j}\} = [B_M]\{\mathbf{M}^I\}. \quad \text{(B7)}$$

The surface traction, normal component of magnetic induction, and the gradient flux of ferromagnetic materials are similarly derived from the interpolation functions and quantities of nodal variables as

$$\{\mathbf{T}\} = [N_T]\{\mathbf{T}^I\}, \quad B_n = \langle N_B\rangle\{B_n^I\}, \quad \{\pi_\mathbf{M}\} = [N_\pi]\{\pi_\mathbf{M}^I\}, \quad \text{(B8)}$$

where $[N_T]$, $\langle N_B\rangle$, and $[N_\pi]$ are interpolation function matrices [35]. Substitution of Eqs. (B6)–(B8) into Eq. (B5), the nonlinear equations in terms of the quantities of nodal variables are obtained:

$$\int_V \{\{\delta\mathbf{u}^I\}^T[B_u]^T[c][B_u]\{\mathbf{u}^I\} - \{\delta\mathbf{u}^I\}^T[B_u]^T[Q][N_M]\{\mathbf{M}^I\} - \{\delta\phi_M^I\}^T[B_\phi]^T[\mu_0][B_\phi]\{\phi_M^I\}.$$

$$\times \{\delta\phi_M^I\}^T[B_\phi]^T[\mu_0][N_M]\{\mathbf{M}^I\} - \{\delta\mathbf{M}^I\}^T[N_M]^T[D1_\gamma][N_M]\{\mathbf{M}^I\} - \{\delta\mathbf{M}^I\}^T[N_M]^T[\mu_\gamma][N_M]\{\mathbf{M}^I\}$$

$$- \{\delta\mathbf{M}^I\}^T[N_M]^T[e_\gamma][N_M]\{\mathbf{M}^I\} + \{\delta\mathbf{M}^I\}^T[N_M]^T[\mathbf{M}_{i,t}] + \{\delta\mathbf{M}^I\}^T[N_M]^T[\alpha][N_M]\{\mathbf{M}^I\}$$

$$+ \{\delta\mathbf{M}^I\}^T[N_M]^T[D1][B_M]\{\mathbf{M}^I\} - \{\delta\mathbf{M}^I\}^T[N_M]^T[\mu][B_\phi]\{\phi_M^I\} + \{\delta\mathbf{M}^I\}^T[N_M]^T[e][B_u]\{\mathbf{u}^I\}$$

$$- \{\delta\mathbf{M}^I\}^T[B_M]^T[A_\gamma][N_M]\{\mathbf{M}^I\} - \{\delta\mathbf{M}^I\}^T[B_M]^T[D2_\gamma][N_M]\{\mathbf{M}^I\} + \{\delta\mathbf{M}^I\}^T[B_M]^T[A][B_M]\{\mathbf{M}^I\}$$

$$+ \{\delta\mathbf{M}^I\}^T[B_M]^T[D2][N_M]\{\mathbf{M}^I\}\}dV = \int_S \{\{\delta\mathbf{u}\}^T\{\mathbf{T}\} + B_n\delta\phi_M + \{\delta\mathbf{M}\}^T\{\pi_\mathbf{M}\}\}dS, \quad \text{(B9)}$$

which can be written as

$$\begin{bmatrix} K_{uu} & 0 & -K_{uM} \\ 0 & -K_{\phi\phi} & K_{\phi M} \\ K_{Mu} & -K_{M\phi} & K_{MM}+K_{D1}+K_{D2}+K_{ex}-K_{D1\gamma}-K_{\mu\gamma}-K_{e\gamma}-K_{A\gamma}-K_{D2\gamma} \end{bmatrix} \begin{Bmatrix} \mathbf{u}^I \\ \phi_M^I \\ \mathbf{M}^I \end{Bmatrix} = \begin{Bmatrix} \mathbf{F}_S \\ \mathbf{B}_S \\ \mathbf{\Pi}_{\mathbf{M}_S} \end{Bmatrix}, \quad \text{(B10)}$$

where

$$[K_{uu}] = \int_V [B_u]^T[c][B_u]dV,$$

$$[K_{uM}] = \int_V [B_u]^T[Q][N_M]dV,$$

$$[K_{\phi\phi}] = \int_V [B_\phi]^T[\mu_0][B_\phi]dV,$$

$$[K_{\phi M}] = \int_V [B_\phi]^T[\mu_0][N_M]dV,$$

$$[K_{Mu}] = \int_V [N_M]^T[e][B_u]dV,$$

$$[K_{M\phi}] = \int_V [N_M]^T[\mu][B_\phi]dV,$$

$$[K_{MM}] = \int_V [N_M]^T[\alpha][N_M]dV,$$

$$[K_{D1}] = \int_V [N_M]^T[D1][B_M]dV,$$

$$[K_{D2}] = \int_V [B_M]^T[D2][N_M]dV,$$

$$[K_{ex}] = \int_V [B_M]^T[A][B_M]dV,$$

$$[K_{D1\gamma}] = \int_V [N_M]^T [D1_\gamma][N_M]dV,$$

$$[K_{\mu\gamma}] = \int_V [N_M]^T [\mu_\gamma][N_M]dV,$$

$$[K_{e\gamma}] = \int_V [N_M]^T [e_\gamma][N_M]dV,$$

$$[K_{A\gamma}] = \int_V [B_M]^T [A_\gamma][N_M]dV,$$

$$[K_{D2\gamma}] = \int_V [B_M]^T [D2_\gamma][N_M]dV,$$

$$\{\mathbf{F}_s\} = \int_S [N_u]^T [N_T]dS\{\mathbf{T}^I\},$$

$$\{\mathbf{B}_s\} = \int_S \langle N_\phi \rangle^T \langle N_B \rangle dS\{B_n^I\},$$

$$\{\mathbf{\Pi_{M_s}}\} = -\int_V [N_M]^T \{\mathbf{M}_{i,t}\}dV + \int_S [N_M]^T [N_\pi]dS\{\pi_\mathbf{M}^I\}. \tag{B11}$$

The equations in Eq. (B10) are a set of nonlinear equations including 56 nodal variables for each element and must be solved by an iteration method. A Newton method [35] is employed to solve these equations. Equation (B10) can be written as

$$\mathbf{R}_i(\mathbf{d}) = 0 \ (i = 1, 2 \dots, 56), \tag{B12}$$

where $\mathbf{d} = \{\mathbf{u}^I \phi_M^I \mathbf{M}^I\}^T$. To implement a Newton method, it is necessary to linearize the residual equations of Eq. (B12). The Newton equation may be written as

$$\mathbf{R}_i^{(k+1)} = \mathbf{R}_i^k + \left.\frac{\partial \mathbf{R}_i}{\partial \mathbf{d}_j}\right|^{(k)} \Delta\mathbf{d}_j^{(k)} = 0. \tag{B13}$$

Equation (B13) becomes a linear equation with new unknown variables $\Delta\mathbf{d}_j^{(k)}$ for given values of $\mathbf{d}$ at previous iterative step k. If we define $S_{ij}^{(k)} = -\frac{\partial \mathbf{R}_i}{\partial \mathbf{d}_j}|^{(k)}$, then Eq. (B13) becomes

$$[S_{ij}^{(k)}]\{\Delta\mathbf{d}_j^{(k)}\} = \{\mathbf{R}_i^k\}. \tag{B14}$$

After finding the solution of Eq. (B14), the values of $\mathbf{d}_j$ at the next iterative step $k + 1$ are updated as

$$\mathbf{d}_j^{(k+1)} = \mathbf{d}_j^{(k)} + \Delta\mathbf{d}_j^{(k)} = 0. \tag{B15}$$

The element tangent matrix is

$$[S_{ij}^{(k)}] = \begin{bmatrix} K_{uu} & 0 & -K_{uM}^S \\ 0 & -K_{\phi\phi} & K_{\phi M} \\ K_{Mu} - K_{e\gamma}^{Su} & -K_{M\phi} - K_{\mu\gamma}^S & K_{Mt}^S + K_{Mu}^S + K_{MM}^S + K_{D1} + K_{D2} + K_{ex} - K_{D1\gamma} \\ & -K_{D1\gamma}^S - K_{\mu\gamma} - K_{e\gamma}^{SM} - K_{A\gamma} - K_{A\gamma}^S - K_{D2\gamma}^S \end{bmatrix}, \tag{B16}$$

where

$$[K_{uM}^S] = \int_V [B_u]^T [Q^S][N_M]dV,$$

$$[K_{Mu}^S] = \int_V [N_M]^T [e^S][N_M]dV,$$

$$[K_{MM}^S] = \int_V [N_M]^T [\alpha^S][N_M]dV,$$

$$[K_{Mt}^S] = \int_V [N_M]^T [\mathbf{M}_{i,t}^S][N_M]dV,$$

$$[K_{D1\gamma}^S] = \int_V [N_M]^T [D1\gamma^S][B_M]dV,$$

$$\left[K_{\mu\gamma}^{S}\right] = \int_{V} [N_M]^T [\mu\gamma^S][B_\phi] dV,$$

$$\left[K_{e\gamma}^{Su}\right] = \int_{V} [N_M]^T [e\gamma^{Su}][B_u] dV,$$

$$\left[K_{e\gamma}^{SM}\right] = \int_{V} [N_M]^T [e\gamma^{SM}][N_M] dV,$$

$$\left[K_{A\gamma}^{S}\right] = \int_{V} [B_M]^T [A\gamma^S][B_M] dV,$$

$$\left[K_{D2\gamma}^{S}\right] = \int_{V} [B_M]^T [D2\gamma^S][N_M] dV. \tag{B17}$$

[1] L. D. Landau and E. M. Lifshitz, *Electrodynamics of Continuous Media* (Pergamon Press, Oxford, 1961).

[2] C. A. Gonano, R. E. Zich, and M. Mussetta, Definition for polarization *p* and magnetization m fully consistent with Maxwell's equations, Prog. Electromagn. Res. B **64**, 83 (2015).

[3] H. J. Williams, R. M. Bozorth, and W. Shockley, Magnetic domain patterns on single crystals of silicon iron, Phys. Rev. **75**, 155 (1949).

[4] U. K. Rößler, A. N. Bogdanov, and C. Pfleiderer, Spontaneous skyrmion ground states in magnetic metals, Nature (London) **442**, 797 (2006).

[5] X. Z. Yu, Y. Onose, N. Kanazawa, J. H. Park, J. H. Han, Y. Matsui, N. Nagaosa, and Y. Tokura, Real-space observation of a two-dimensional skyrmion crystal, Nature (London) **465**, 901 (2010).

[6] S. Woo, K. Litzius, B. Krüger, M. Y. Im, L. Caretta, K. Richter, M. Mann, A. Krone, R. M. Reeve, M. Weigand *et al.*, Observation of room-temperature magnetic skyrmions and their current-driven dynamics in ultrathin metallic ferromagnets, Nat. Mater. **15**, 501 (2016).

[7] S. Krause and R. Wiesendanger, Spintronics: Skyrmionics gets hot, Nat. Mater. **15**, 493 (2016).

[8] S. Luo, Y. Zhang, M. Shen, J. Ou-Yang, B. Yan, X. Yang, S. Chen, B. Zhu, and L. You, Skyrmion-based high-frequency signal generator, Appl. Phys. Lett. **110**, 112402 (2017).

[9] M. Mochizuki and S. Seki, Magnetoelectric resonances and predicted microwave diode effect of the skyrmion crystal in a multiferroic chiral-lattice magnet, Phys. Rev. B **87**, 134403 (2013).

[10] T. L. Gilbert, A phenomenological theory of damping in ferromagnetic materials, IEEE Trans. Magn. **40**, 3443 (2004).

[11] L. Landau and E. Lifshitz, On the theory of the dispersion of magnetic permeability in ferromagnetic bodies, Phys. Z. Sowjet. **8**, 153 (1935).

[12] M. Lakshmanan and K. Nakamura, Landau-Lifshitz Equation of Ferromagnetism: Exact Treatment of the Gilbert Damping, Phys. Rev. Lett. **53**, 2497 (1984).

[13] M. Yi and B. X. Xu, A constraint-free phase field model for ferromagnetic domain evolution, Proc. R. Soc. A **470**, 20140517 (2014).

[14] J. X. Zhang and L. Q. Chen, Phase-field microelasticity theory and micromagnetic simulations of domain structures in giant magnetostrictive materials, Acta Mater. **53**, 2845 (2005).

[15] B. Yang and D. R. Fredkin, Dynamical micromagnetics by the finite element method, IEEE Trans. Magn. **34**, 3842 (1998).

[16] C. Miehe and G. Ethiraj, A geometrically consistent incremental variational formulation for phase field models in micromagnetics, Comput. Methods Appl. Mech. Eng. **245–246**, 331 (2012).

[17] J. M. Hu, G. Sheng, J. X. Zhang, C. W. Nan, and L. Q. Chen, Phase-field simulation of strain-induced domain switching in magnetic thin films, Appl. Phys. Lett. **98**, 112505 (2011).

[18] H. Szambolics, L. D. Buda-Prejbeanu, J. C. Toussaint, and O. Fruchart, A constrained finite element formulation for the Landau-Lifshitz-Gilbert equations, Comput. Mater. Sci. **44**, 253 (2008).

[19] F. Alouges and P. Jaisson, Convergence of a finite element discretization for the Landau-Lifshitz equations in micromagnetism, Math. Models Methods Appl. Sci. **16**, 299 (2006).

[20] G. Ethiraj and C. Miehe, A projection method for phase field models in micromagnetics, Proc. Appl. Math. Mech. **12**, 399 (2012).

[21] A. O. Leonov and A. N. Bogdanov, Crossover of skyrmion and helical modulations in noncentrosymmetric ferromagnets, New J. Phys. **20**, 43017 (2018).

[22] E. Moskvin, S. Grigoriev, V. Dyadkin, H. Eckerlebe, M. Baenitz, M. Schmidt, and H. Wilhelm, Complex Chiral Modulations in FeGe Close to Magnetic Ordering, Phys. Rev. Lett. **110**, 077207 (2013).

[23] H. Wilhelm, M. Baenitz, M. Schmidt, U. K. Rößler, A. A. Leonov, and A. N. Bogdanov, Precursor Phenomena at the Magnetic Ordering of the Cubic Helimagnet FeGe, Phys. Rev. Lett. **107**, 127203 (2011).

[24] U. Atxitia, D. Hinzke, and U. Nowak, Fundamentals and applications of the Landau-Lifshitz-Bloch equation, J. Phys. D: Appl. Phys. **50**, 033003 (2017).

[25] D. A. Garanin, Fokker-Planck and Landau-Lifshitz-Bloch equations for classical ferromagnets, Phys. Rev. B **55**, 3050 (1997).

[26] D. A. Garanin and O. Chubykalo-Fesenko, Thermal fluctuations and longitudinal relaxation of single-domain magnetic particles at elevated temperatures, Phys. Rev. B **70**, 212409 (2004).

[27] R. F. L. Evans, D. Hinzke, U. Atxitia, U. Nowak, R. W. Chantrell, and O. Chubykalo-Fesenko, Stochastic form of the Landau-Lifshitz-Bloch equation, Phys. Rev. B **85**, 014433 (2012).

[28] D. Hinzke and U. Nowak, Domain Wall Motion by the Magnonic Spin Seebeck Effect, Phys. Rev. Lett. **107**, 027205 (2011).

[29] S. M. Allen and J. W. Cahn, A microscopic theory for antiphase boundary motion and its application to antiphase domain coarsening, Acta Metall. **27**, 1085 (1979).

[30] A. Gordon, I. D. Vagner, and P. Wyder, Kinetics of diamagnetic phase transitions, Phys. Rev. B **41**, 658 (1990).

[31] C. M. Landis, A continuum thermodynamics formulation for micro-magneto-mechanics with applications to ferromagnetic shape memory alloys, J. Mech. Phys. Solids **56**, 3059 (2008).

[32] Y. Wang and J. Wang, The temperature-strain phase diagrams of ferromagnetic thin films under different magnetic fields, J. Phys.: Condens. Matter **33**, 235802 (2021).

[33] Y. Wang, T. Shimada, J. Wang, T. Kitamura, and H. Hirakata, The rectilinear motion of the individual asymmetrical skyrmion driven by temperature gradients, Acta Mater. **221**, 117383 (2021).

[34] Y. Wang, J. Sun, T. Shimada, H. Hirakata, T. Kitamura, and J. Wang, Ferroelectric control of magnetic skyrmions in multiferroic heterostructures, Phys. Rev. B **102**, 014440 (2020).

[35] J. Wang and J. Zhang, A real-space phase field model for the domain evolution of ferromagnetic materials, Int. J. Solids Struct. **50**, 3597 (2013).

[36] Y. Ni, L. He, and A. G. Khachaturyan, Equivalency principle for magnetoelectroelastic multiferroics with arbitrary microstructure: the phase field approach, J. Appl. Phys. **108**, 023504 (2010).

[37] X. Lu, H. Li, and B. Wang, Theoretical analysis of electric, magnetic and magnetoelectric properties of nano-structured multiferroic composites, J. Mech. Phys. Solids **59**, 1966 (2011).

[38] M. Lakshmanan, The fascinating world of the Landau-Lifshitz-Gilbert equation: An overview, Philos. Trans. R. Soc. A **369**, 1280 (2011).

[39] I. Dzyaloshinsky, A thermodynamic theory of "weak" ferromagnetism of antiferromagnetics, J. Phys. Chem. Solids **4**, 241 (1958).

[40] T. Moriya, Anisotropic superexchange interaction and weak ferromagnetism, Phys. Rev. **120**, 91 (1960).

[41] Y. Hu and B. Wang, Unified theory of magnetoelastic effects in B20 chiral magnets, New J. Phys. **19**, 123002 (2017).

[42] J. M. Porro, A. Bedoya-Pinto, A. Berger, and P. Vavassori, Exploring thermally induced states in square artificial spin-ice arrays, New J. Phys. **15**, 055012 (2013).

[43] B. Sarkar, B. Dalal, V. Dev Ashok, K. Chakrabarti, A. Mitra, and S. K. De, Magnetic properties of mixed spinel $BaTiO_3 - NiFe_2O_4$ composites, J. Appl. Phys. **115**, 123908 (2014).

[44] R. G. Harrison, Calculating the spontaneous magnetization and defining the curie temperature using a positive-feedback model, J. Appl. Phys. **115**, 033901 (2014).

[45] S. Mühlbauer, B. Binz, F. Jonietz, C. Pfleiderer, A. Rosch, A. Neubauer, R. Georgii, and P. Böni, Skyrmion lattice in a chiral magnet, Science **323**, 915 (2009).

[46] C. Pfleiderer, D. Reznik, L. Pintschovius, H. V. Löhneysen, M. Garst, and A. Rosch, Partial order in the non-fermi-liquid phase of MnSi, Nature (London) **427**, 227 (2004).

[47] A. Vansteenkiste, J. Leliaert, M. Dvornik, M. Helsen, F. Garcia-Sanchez, and B. Van Waeyenberge, The design and verification of MUMAX3, AIP Adv. **4**, 107133 (2014).

[48] R. Tomasello, E. Martinez, R. Zivieri, L. Torres, M. Carpentieri, and G. Finocchio, A strategy for the design of skyrmion racetrack memories, Sci. Rep. **4**, 6784 (2014).

[49] A. A. Thiele, Steady-State Motion of Magnetic Domains, Phys. Rev. Lett. **30**, 230 (1973).

[50] D. Capic, D. A. Garanin, and E. M. Chudnovsky, Skyrmion-skyrmion interaction in a magnetic film, J. Phys.: Condens. Matter **32**, 415803 (2020).

[51] S.-Z. Lin, C. Reichhardt, C. D. Batista, and A. Saxena, Particle model for skyrmions in metallic chiral Magnets: Dynamics, Pinning, and creep, Phys. Rev. B **87**, 214419 (2013).

[52] D. Cortés-Ortuño, W. Wang, M. Beg, R. A. Pepper, M. A. Bisotti, R. Carey, M. Vousden, T. Kluyver, O. Hovorka, and H. Fangohr, Thermal stability and topological protection of skyrmions in nanotracks, Sci. Rep. **7**, 4060 (2017).

[53] See Supplemental Material at http://link.aps.org/supplemental/10.1103/PhysRevB.106.094423 for more information concerning curves, the precursor effect, and magnetic domain structure.

[54] V. Z. C. Paes, J. Varalda, and D. H. Mosca, Strain-induced magnetization changes and magneto-volume effects in ferromagnets with cubic symmetry, J. Magn. Magn. Mater. **475**, 539 (2019).

[55] T. Meier, *Ferromagnetische Resonanz (FMR)* (Technische Universität München, Fortgeschrittenenpraktikum, 2020).

[56] G. Woltersdorf, *Spin-Pumping and Two-Magnon Scattering in Magnetic Multilayers*, Ph.D. thesis (Martin-Luther-Universität, Halle, 2001).

[57] J. M. Hu, T. Yang, and L. Q. Chen, Stability and dynamics of skyrmions in ultrathin magnetic nanodisks under strain, Acta Mater. **183**, 145 (2020).

[58] J. Miltat, S. Rohart, and A. Thiaville, Brownian motion of magnetic domain walls and skyrmions, and their diffusion constants, Phys. Rev. B **97**, 214426 (2018).

[59] Y. Wang, T. Kitamura, J. Wang, H. Hirakata, and T. Shimada, Mechanical Acceleration and Control of the Thermal Motion of a Magnetic Skyrmion, Phys. Rev. Appl. **18**, 014049 (2022).